

Article

Interaction of Model Inhibitor Compounds with Minimalist Cluster Representations of Hydroxyl Terminated Metal Oxide Surfaces

Christopher D. Taylor ^{1,*}, Yathish Kurapati ² and Sujit K. Mondal ³

¹ DNV GL, 5777 Frantz Rd, Dublin, OH 43017, USA

² Institute for Corrosion and Multiphase Technology, Ohio University, Athens, OH 45701, USA; yk935214@ohio.edu

³ Corrosion Technology Program, Material Science Center of Excellence, Houston, TX 77087, USA; sujit.mondal@hccs.edu

* Correspondence: christopher.taylor@dnvgl.com

Received: 22 December 2017; Accepted: 12 January 2018; Published: 23 January 2018

Abstract: The computational modeling of corrosion inhibitors at the level of molecular interactions has been pursued for decades, and recent developments are allowing increasingly realistic models to be developed for inhibitor–inhibitor, inhibitor–solvent and inhibitor–metal interactions. At the same time, there remains a need for simplistic models to be used for the purpose of screening molecules for proposed inhibitor performance. Herein, we apply a reductionist model for metal surfaces consisting of a metal cation with hydroxide ligands and use quantum chemical modeling to approximate the free energy of adsorption for several imidazoline class candidate corrosion inhibitors. The approximation is made using the binding energy and the partition coefficient. As in some previous work, we consider different methods for incorporating solvent and reference systems for the partition coefficient. We compare the findings from this short study with some previous theoretical work on similar systems. The binding energies for the inhibitors to the metal hydroxide clusters are found to be intermediate to the binding energies calculated in other work for bare metal vs. metal oxide surfaces. The method is applied to copper, iron, aluminum and nickel metal systems.

Keywords: quantum chemistry; adsorption energy; partition coefficient; computational design; corrosion inhibitors

1. Introduction

Corrosion inhibitors, as defined by Obot [1], are substances that “when added in a small concentration to an environment effectively [reduce] the corrosion rate of a metal exposed to that environment”. Corrosion inhibitors are utilized heavily in oil and gas exploration and production, water treatment and power generation industries [2]. Due to the commercial market for inhibitors, roughly \$2.5 bn estimated for 2017 in the US [1], there is a competitive drive to develop new inhibitors with better performance. Furthermore, for the sake of asset management and reducing the health, safety and environmental impacts of industrial practice, it is of importance to develop science-based models for assessing and predicting the extent and longevity of action for those corrosion inhibitors which are deployed [3]. For these reasons, the computational modeling of inhibitors, and particularly computationally assisted inhibitor design, has been an intensive area of research for the past few decades [4].

Computational modeling of inhibitors can provide several useful purposes:

- a. Providing a framework for understanding the science of how functionality and tail groups influence different aspects of the inhibition process [3]

- b. Serving as a component of an engine for design of new inhibitors (i.e., high throughput computational design) [5,6]
- c. Prediction of effectiveness of corrosion mitigation given an environment, metal surface to protect and an inhibitor compound [7]

Currently, computational modeling of inhibitors falls mostly into category (a) and also partly in category (b). Accomplishing purpose (c) requires a multiphysics paradigm that is still under active development [3].

Many efforts have been made to accomplish purpose (b) using the quantitative structure active relations (QSAR) technique, which have undergone many iterations as different molecular properties become calculable with the maturation of quantum chemical codes [8–12]. For example, modern QSAR approaches can now include many variables including adsorption energies and Fukui functions, whereas the earlier approaches focused only on the energies of the frontier orbitals (E_{HOMO} , E_{LUMO}), etc. [13]. They also may use support vector machines (SVM) [14] or deep neural networks [7] in place of linear regressions to inhibitor efficiencies obtained from experiment. The increasing utility of data analytics can be anticipated to drive further revolutions in this approach, which primarily uses regression and correlations to define relations between molecular descriptors and inhibitor performance under various conditions. Furthermore, molecular modeling tools that can incorporate dynamics and realistic models for metallic and/or oxidized surfaces like LAMMPS [15], and VASP [16–18] are now expanding what is possible under purpose (a), since now metal surfaces can be modeled with great fidelity, with the emphasis now being placed on trying to better model defects and passive films, as well as the electrochemical environment [14,19,20]. Descriptors derived from these calculations can be applied into mechanistic based models or into the data analytic type approaches, such as QSAR [8], SVM [14] and the use of deep neural networks [7].

It was observed in the work of Mondal and Taylor that there is no consensus for a strong correlation between an individual molecular parameter and corrosion efficiency of an inhibitor compound [21]. A similar observation regarding the limit of “molecule-only” descriptors and QSAR models was made by Kokalj [22]. This challenge was attributed to several factors, including the variations that can result in measured corrosion inhibitor efficiencies due to differences in surface handling and solution preparation, as well as the interactions between molecular parameters and metallic surface parameters such as proportion of defect sites on the surface, surface crystallographic orientation, microstructure and processing relations, etc. Furthermore, using an empirical correlation approach alone does not lend itself to extrapolations; for this, a science based model is required that considers the various processes that result in the direct or indirect inhibition of corrosion reactions [3]. Despite this assertion, some considerable recent success has been made by Winkler et al. [23,24] and Chen et al. [25,26] to use advanced machine learning methods to correlate a variety of molecular descriptors to different observable indicators of corrosion protection (such as corrosion current density, corrosion potential, and the anodic and cathodic Tafel slopes), and then to integrate these findings within a multiphysics model for microclimate exposure performance in aluminum alloy systems.

A combination of the two approaches (empirical and science-based) was developed by Mondal and Taylor [21]. The model uses small metal hydroxide “clusters” to simulate the chemistry of a hydroxylated passive film, and their interactions with organic molecules. The adsorption energy of candidate inhibitor molecules to the clusters was determined using density functional theory (DFT) and related to the enthalpy for binding. The $\log P$ parameter (i.e., the partition coefficient [27]) for the candidate molecule was also calculated using solvation free energy models and related to the entropy of binding. The two terms were then used to calibrate a QSAR type model for the inhibitor efficiency. This model is attractive for several reasons. First, it uses a model that is computationally inexpensive compared to more comprehensive models of the metal surface; second, the model is potentially more realistic as many metallic surfaces in practice will not be bare on the metallic surface at the atomic level, but instead contain some extent of oxide or hydroxylation. Third, it does not rely on finding correlations between molecular descriptors in isolation of an environment as in the QSAR

and machine learning approaches, but can include the effects of solvation and surface binding, as well as be varied according to the type of metal surface encountered. Finally, it employs some physics in terms of relating the computed parameters directly to the free energy required to adsorb the inhibitor molecule to the surface to be protected.

Only a few theoretical studies have focused directly on the interaction of inhibitor molecules with oxidized surfaces. The interactions of imidazoline with Fe, Fe₂O₃ and Fe₃O₄ surfaces were studied using classical molecular dynamics [28]. The imidazoline adsorbed in these calculations with a flat geometry and large adsorption energies determined as −284, −226 and −157 kJ/mol for the three surfaces, respectively. The use of classical molecular dynamics (MD), such as the COMPASS forcefield, however, means that the energies may not be accurate, as very few potentials accurately model surface/molecule interactions. The interactions of thiazoles with Cu₂O(111) were studied using local density approximation (LDA) DFT (adsorption energies of −1.43 eV or −3.07 eV at low or high coverage were reported) [29], as were the adsorption of glycine and methylamine on Al₂O₃ [30,31], glycine on AlOOH [32], and various organic acids on ZnO(0001) with adsorption energies reported in a range from −2.3 to −2.8 eV depending on the size of the carbon chain [33–36]. Some more complex DFT calculations have examined inhibitor adsorption on metallic and oxidized surfaces in the presence of solvent and electrochemical double layer effects [37]. Kokalj and co-workers have investigated using DFT methods the interaction of benzotriazole molecule with Cu₂O surface [38]. Two types of surface diagrams were investigated (i) Cu₂O coordinatively saturated (CSA) and (ii) coordinatively unsaturated (CUS). Neutral benzotriazole binds weakly with saturated copper surface compared to the unsaturated Cu-surface. A comparison between the current study and previous DFT studies of benzotriazole on metallic Cu surfaces reveals that the bonding of benzotriazole to Cu₂O surfaces is not very different from that on metallic Cu surfaces, although some differences are significant. Neutral BTAH binds considerably more strongly to Cu-unsaturated center sites on Cu₂O(111) than to metallic Cu surfaces, but deprotonated BTA binds significantly less strongly to coordinatively saturated Cu sites on Cu₂O surfaces than to metallic Cu surfaces. This article suggests that binding energy with unsaturated Cu surface is so strong that it overcompensates for a thermodynamic deficiency of stoichiometric ratio for Cu₂O. The impact of van der Waals dispersion interactions on adsorption bonding was also addressed, and their main effect is to strengthen the molecule–surface bonding; this observation matches with the article published by Mondal and Taylor [21]. The binding energies reported for BTAH to the Cu₂O surface range from −0.4 to −0.7 eV (for oxygen terminated surface), to −1.5 eV to uncoordinated Cu atoms and as much as −1.7 to −2.0 eV and −2.8 eV for the deprotonated form on the saturated and unsaturated sites, respectively. When compared to the study of azoles on Cu(111) and Al(111), the binding energies are significantly stronger for the oxide surface, with binding energies between −0.22 and −0.69 eV for the metallic surfaces (weaker binding for azole rings with more N atoms substituting for C) [39].

In the present paper, we further investigate the utility of the model initially introduced by Mondal and Taylor by extending to some other metal centers such as Al(OH)₃, Cu(OH)₂, Ni(OH)₂ and Fe(OH)₂. The approach is complementary to some of the DFT approaches, for example those of Kokalj or Costa [37,38], that modeled adsorption on metallic surfaces. It has been noted that discrepancies between adsorption energies and actually reported inhibitor performance may be due to neglecting the oxidized or partially oxidized surface. Hence, we study the adsorption interaction between metal ion clusters with hydroxide and a series of inhibitors based on imidazole functionality for the metals Ni, Cr, Fe, and Al. Not only can hydroxides model the hydroxylated surfaces of an oxide film under acidic conditions, but they can also model low-coordinated defect sites, and/or corrosion products. The data produced in this paper, therefore, can be used in a broader multiphysics model that includes these effects as well as other phenomena such as partitioning, protonation effects, micelle formation, fluid dynamics, etc. [3].

2. Computational Methods

Adsorption of molecules on solid surfaces is favored when the overall free energy of the system (ΔG) decreases upon adsorption [40]. The equilibrium constant for adsorption, K , is given by the free energy relation:

$$K = e^{-\frac{\Delta G_0^{ads}}{RT}}. \quad (1)$$

It is commonly assumed that the inhibition efficiency η will be proportional to the equilibrium constant. A more detailed understanding of the formation of monolayers, bilayers, etc. on the surface of the material and their ability to inhibit the corrosion reactions on the surface as well as the mass transport across the double layer would be required to further explore the relations between the equilibrium constant and the inhibition efficiency [3]. However, if we take this simple assumption, i.e., that inhibitor efficiency will increase with a stronger binding of the inhibitor compound to the surface, approximating ΔG_0^{ads} from first-principles will allow comparison of model inhibitor molecules to one another, and differences in expected efficiencies for different types of materials. In the present work, the DFT-based computational model developed by Mondal and Taylor is employed to approximate the free energy of adsorption by calculating the binding energy of imidazolium type corrosion inhibitors with irreducible representations of metal hydroxides [21].

The different inhibitors employed in this study are shown in Figure 1. As imidazoles are used in a variety of applications, we study imidazole and some of its derivatives: methylimidazole, benzimidazole, L-histidine, and two long-chain imidazolines (with C₁₄ and C₁₆ tails). In this way, we can explore the role of functionalization, as well as the variation in metal center.

The change in enthalpy of adsorption in this work will be approximated by the difference in self-consistent DFT energies obtained from the electronic structure calculations [41]. There is an entropic factor that is also involved in the adsorption process—an inhibitor in the bulk system is surrounded by a cage of solvent molecules that will need to be ruptured, at least in part depending on the nature of the inhibiting film that forms, for it to adsorb on the metal. In addition, the water molecules on the surface shall be displaced and, once adsorbed, both the inhibitor molecules and solvent will have reduced degrees of freedom. All these factors will affect the entropy of solvent and inhibitor, which can either positively or negatively contribute to the overall change in free energy. The change in entropy is approximated as a function of the hydrophobicity of the inhibitor molecule, which is expressed as $(R \log P)$, where P represents the partition coefficient (nominally, this is reported with respect to *n*-octanol, although herein we will consider other potential solvents) and R is the universal gas constant. Under this interpretation, molecules with a high hydrophobicity will have a higher value for $\log P$, and, furthermore, will have a more positive change in entropy associated with adsorption. We can express these contributions and our approximations mathematically below:

$$\Delta G_{ads}^0 = \Delta H_{ads}^0 - T \Delta S_{ads}^0 \quad (2)$$

$$\Delta G_{ads}^0 \cong E_{ads} - RT * (\log P). \quad (3)$$

All the calculations were performed with Gaussian 09W [42] on a desktop workstation with two Intel Xeon E5-2697 processors (24 cores and 2.7 GHz base frequency). As discussed by Mondal et al., a small cluster model of inorganic metal hydroxide is considered as a proxy for an oxide covered metal surface [21]. Self-consistent field (SCF) energies for the inhibitor, metal hydroxide (substrate) and the inhibitor+substrate complex were calculated after optimizing the respective molecular geometries. B3LYP functional [43] and LaNL2DZ basis sets [44–46] were used for geometry optimization, whereas the single point energies (SPE) of the optimized molecules were calculated using the M06 functional [47–49] and 6-311G+(d,p) basis sets. The adsorption energies were obtained using the following expression:

$$E_{ads} = (SCF_{inhibitor} + SCF_{substrate}) - SCF_{inhibitor+substrate} \quad (4)$$

The adsorption energy so determined will depend on the binding mode being considered. For simplicity as well as consistency between the metal centers and molecules considered, all the calculations were performed assuming the metal atom binds to the unsaturated nitrogen on the imidazole ring. Molecular dynamics studies by Feng et al. [28] and Ramachandran and Jovancicevic [50] as well as some experimental studies using the SERS technique (surface enhanced Raman spectroscopy) [51] have shown that ring structures like imidazolines may also bind in a flat or slightly tilted orientation whereby the π -aromaticity of the imidazole group and/or phenyl groups (in the case of benzimidazole) can donate electron density to the surface. However, given the reductionist nature of the present model, we do not consider that orientation. In addition, the challenges to constructing adequate force fields for solid/liquid interfaces used in the MD studies [52], and the assignments of orientations based on SERS spectra [53,54], may not be completely definitive as to proving that the flat orientation is preferred. Furthermore, the investigation of Kovacevic et al. using the dispersion corrected function PBE + D showed that the zero tilt (i.e., normal orientation as closest to what we have simulated herein) system for imidazole was the lowest energy case on Cu(111) [55]. The binding modes considered are shown in Figure 2 for some of the model systems considered herein.

Partition coefficient represents the ability of an organic molecule to partition between a solvent phase and aqueous phase. For the purpose of estimating the entropy of adsorption, it would be useful to consider partitioning into a phase that resembles the particular environment of the inhibitor surface films that occurs upon adsorption. Traditionally, the partition coefficient is defined as partitioning between *n*-octanol phase and aqueous phase. For inhibitor molecules that have a similar size and structure to *n*-octanol, this may be sufficient. However, it is a topic that could be considered in more detail. Understanding partitioning has also been suggested to be of utility to the availability of chemical inhibitors used in systems of mixed oil and water (i.e., crude oil flow in pipelines, for example) [56]. Considering the application of corrosion inhibitors in crude oil pipelines, it is relevant to look at the partitioning with respect to a solvent having similar characteristics as crude oil. Dielectric constant is one of the critical factors that affect a solvent's ability to contain organic molecules. Hence, a partition coefficient is also calculated with respect to hexane, which has a dielectric constant that is representative of most crude oils. In this study, the partition coefficient was calculated using the expression:

$$\log P = -\frac{\Delta\Delta G_w^0}{RT}, \quad (5)$$

$$\text{where, } \Delta\Delta G_w^0 = \Delta G_{sol}^0 - \Delta G_{sol}^w. \quad (6)$$

The two terms on the right-hand side represent the free energy of solvation of the inhibitor molecule in oil (o) (either *n*-octanol or hexane) and water (w), respectively. By comparing the log *P* predictions for hexane with those obtained for *n*-octanol, we were able to provide some indication of how the entropic terms as well as partitioning behavior might be influenced by only considering the "standard" approach to log *P*, which is based on *n*-octanol. The solvation energies were determined using the SMD implicit solvation method that is available in Gaussian-09W [57].

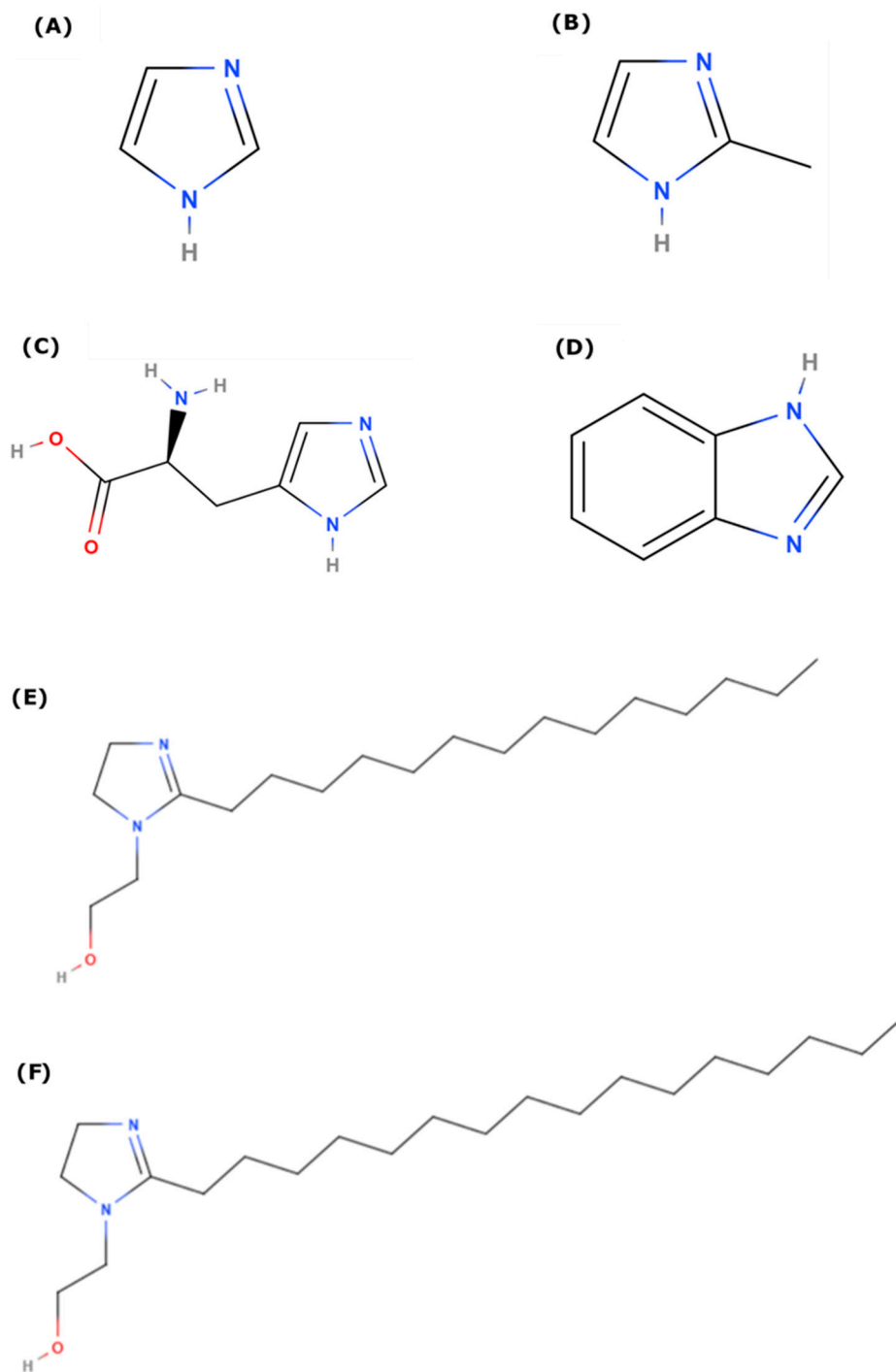


Figure 1. Molecular structure of different imidazole and imidazoline derivatives considered for this study (A) Imidazole (IMZ); (B) 2-Methyl Imidazole (Me-IMZ); (C) L-Histidine (L-HIS); (D) Benzimidazole (BI); (E) Imidazoline based surfactant with $-(\text{CH}_2)_{13}\text{CH}_3$ as tail (IMZ_C14); (F) Imidazoline based surfactant with $-(\text{CH}_2)_{15}\text{CH}_3$ as tail (IMZ_C16).

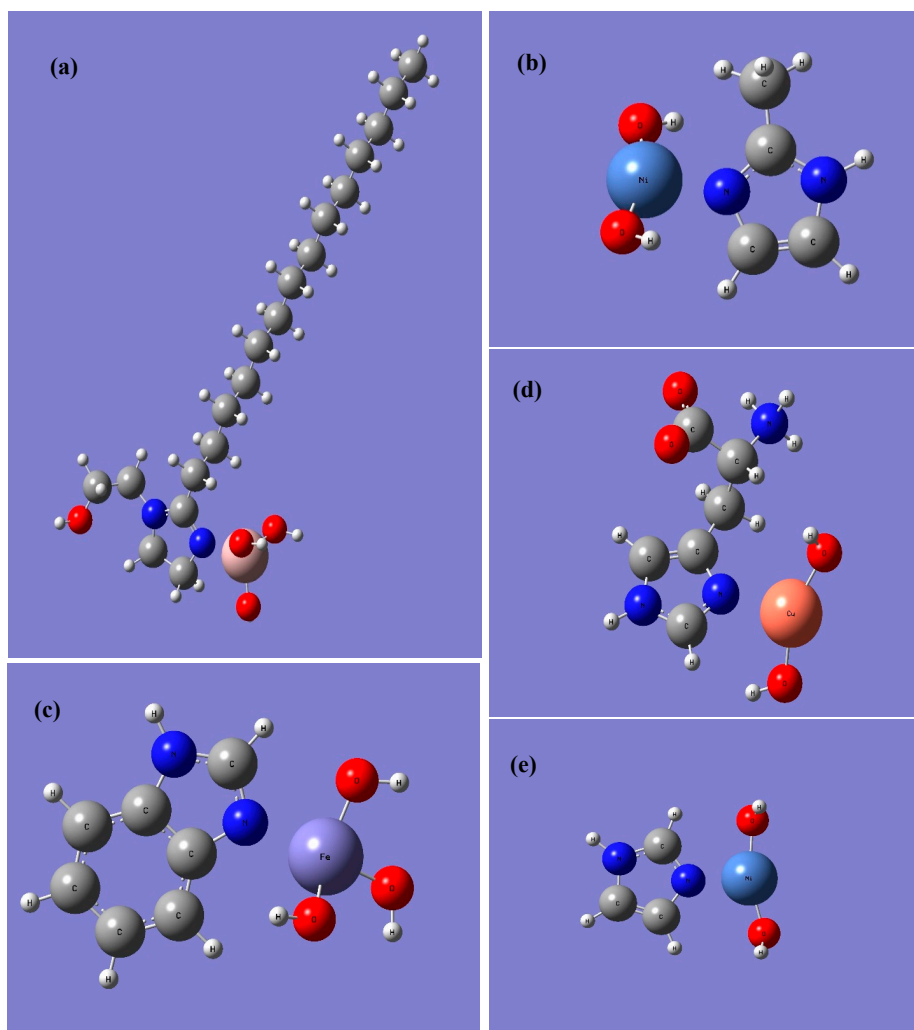


Figure 2. Binding Modes of different inhibitors onto different metal hydroxides (a) optimized structure of IMZ_C14: Al(OH)₃; (b) optimized structure of Me-IMZ: Ni(OH)₂; (c) optimized structure of BI: Fe(OH)₃; (d) optimized structure of L-HIS: Cu(OH)₂; (e) optimized structure of IMZ: Ni(OH)₂.

3. Results

Using the above methodology, the adsorption of the various imidazolium type inhibitors onto Fe(OH)₃, Al(OH)₃, Ni(OH)₂ and Cu(OH)₂ were explored. All the calculated adsorption energies and the hydrophobicity parameters are shown in Tables 1–3. By default, all the energy calculations in Gaussian-09W are done in vacuum without considering any external interactions. However, practically, solvent plays a crucial role in inhibitor adsorption—hence binding energy calculations in the presence of water using an implicit solvation model may be more relevant and are shown in Table 2. The free energies of adsorption calculated as per Equation (3) are shown in Tables 4 and 5.

Table 1. Calculated Binding Energy of different corrosion inhibitors onto various metal hydroxide substrates in the absence of any external interaction.

Metal Hydroxide	Binding Energy in Vacuum (kJ/mol)					
	Corrosion Inhibitor					
	IMZ (A)	Me-IMZ (B)	BI (C)	L-HIS (D)	IMZ_C14 (E)	IMZ_C16 (F)
Cu(OH) ₂	103	110	107	92	125	125

Table 1. Cont.

Metal Hydroxide	Binding Energy in Vacuum (kJ/mol)					
	Corrosion Inhibitor					
	IMZ (A)	Me-IMZ (B)	BI (C)	L-HIS (D)	IMZ_C14 (E)	IMZ_C16 (F)
Fe(OH) ₃	139	157	146	158	–	–
Al(OH) ₃	148	163	152	189	195	195
Ni(OH) ₂	176	186	183	209	202	200

From Table 1, it is evident that inhibitors bind to nickel hydroxide better than other metals considered, for all of the inhibitors studied. Note that the C₁₄ and C₁₆ substituted imidazolines could not be converged for the Fe(OH)₃ case due to issues with obtaining a stable solution to the electronic structure problem that we were unable to solve within the project timeline. Likewise, copper hydroxide has the weakest binding energy than the other metals. Aluminum and iron have similar tendencies, although the binding is stronger to Al(OH)₃ than Fe(OH)₃. The binding energies are of a similar strength, between 92 and 209 kJ/mol. The strongest binding interaction observed here is between L-histidine and nickel hydroxide, whereas the weakest is that between L-histidine and copper hydroxide. The binding energies for C₁₄ and C₁₆ imidazolines are essentially indistinguishable, within the level of chemical accuracy, indicating that any differentiation between performance of those inhibitors must be due to the entropic effect, or potentially molecular packing in the monolayer and/or bilayer films. In all cases, benzimidazole and methyl imidazole are slightly stronger binding inhibitors than imidazole, with benzimidazole being the strongest of the three. For Fe, Al, and Ni, L-histidine is substantially more effective, whereas, for Cu, it is substantially less effective. A more detailed examination of the electronic structure and properties (i.e., hardness, electronegativity, electrostatic potential, etc.) would be required to assess the theoretical reasons underlying these trends.

Table 2. Calculated Binding Energy of different corrosion inhibitors onto various metal hydroxide substrates in the presence of water.

Metal Hydroxide	Binding Energy in Presence of Water (kJ/mol)					
	Corrosion Inhibitor					
	IMZ (A)	Me-IMZ (B)	BI (C)	L-HIS (D)	IMZ_C14 (E)	IMZ_C16 (F)
Cu(OH) ₂	87	91	84	88	95	97
Fe(OH) ₃	81	89	78	97	–	–
Al(OH) ₃	152	161	151	165	177	183
Ni(OH) ₂	169	172	165	177	178	180

Table 2 presents the same adsorption energies as shown in Table 1, but calculated in the presence of an implicit solvent medium (water). The effect of solvation varies according to the metal ion considered. For Cu(OH)₂, the binding energies are weakened by 10–30 kJ/mol, depending on the inhibitor. For Fe(OH)₃, the binding energies are weakened by about 50–60 kJ/mol. For Al(OH)₃, the binding energies vary only slightly by 5–10 kJ/mol, sometimes stronger and sometimes weaker. For Ni(OH)₂, the binding energies are weaker by around 8–20 kJ/mol. Generally, including the effect of hydration seems to have only a slight impact on the calculated adsorption energies, with the exception of Fe(OH)₃, which should be investigated further. The general observation of weaker binding is associated with the net decrease in solvation accessible area, particularly considering that the area no longer available to the solvent after binding is associated with the chemically active sites of the metal hydroxide complex and the inhibitor molecule, which would be most attractive to interactions with water molecules. Including solvation also creates a slightly greater distinction in the binding energies between the C₁₄ and C₁₆ imidazoline groups, presumably due to the effect of the difference in hydrophobicity between the two molecules on the enthalpy of solvation.

Table 3. Calculated values of log *P* using free energy of solvation.

Corrosion Inhibitor	Hydrophobicity (log <i>P</i>)	
	with Reference to <i>n</i> -Octanol	with Reference to Hexane
IMZ (A)	0.04	−4.2
Me-IMZ (B)	−0.16	−5.28
BI (C)	1.73	−2.02
L-His (D)	−3.76	−16.31
IMZ_C14 (E)	11.26	2.73
IMZ_C16 (F)	13.62	6.1

In Table 3, we present the log *P* values as computed for two different reference solvents (*n*-octanol vs. hexane). The partition coefficients in all cases are considerably higher for *n*-octanol, with the highest values observed for C₁₄ and C₁₆ chains of imidazoline. In both cases the trends are the same. Negative log *P* values indicate a preference for the molecule to dissolve in water, whereas positive log *P* values indicate that the molecule will be more likely to dissolve in the solvent. Thus, functionalization of imidazole by methyl or histidine makes it more water soluble, as compared to *n*-octanol. On the other hand, with respect to hexane, all but the very long chains are water soluble. This is insightful with respect to the hydrophobicity and its impact on the entropy of adsorption. According to this theory, the entropy of adsorption should be more favorable for C₁₆ > C₁₄ >> benzimidazole > imidazole > methylimidazole > L-histidine. If the environment of the inhibitor/metal interface is more hydrophobic (i.e., more like hexane than *n*-octanol), then the impact of this entropic differentiation will be more pronounced. Likewise, there will be impacts on the inhibitor availability in a mixed hydrocarbon/water environment, such as in oil and gas pipeline systems.

Table 4. Free Energy of adsorption (kJ/mol) of different corrosion inhibitors on to various metal hydroxide substrates at 298 K in presence of water. Binding Energies from Table 2 and log *P* values with reference to *n*-octanol from Table 3 are used.

Metal Hydroxide	Free Energy of Adsorption at 298 K (kJ/mol)					
	IMZ (A)	Me-IMZ (B)	BI (C)	L-HIS (D)	IMZ_C14 (E)	IMZ_C16 (F)
Cu(OH) ₂	−88	−91	−88	−79	−122	−131
Fe(OH) ₃	−81	−88	−83	−87	−	−
Al(OH) ₃	−152	−161	−155	−156	−205	−217
Ni(OH) ₂	−169	−172	−169	−168	−206	−214

Using the relations for enthalpy and entropy of adsorption as described in the methods section, it is possible to approximate the free energy of adsorption for the inhibitors on the different metal centers. In Table 4, we present the free energies of adsorption at 298 K using the calculated binding energies obtained in the presence of implicit solvent (water), and the partition coefficients determined using the *n*-octanol reference state. In this table, it is clear that, in all cases, the free energy of adsorption is negative, significantly more so for the long chain inhibitors, and less so for the cases of the copper and iron hydroxides. Including the entropic configuration changes the order of preference from the case where only enthalpies are considered. For example, in the case of nickel hydroxide, binding strength varies as BI < IMZ < Me-IMZ < L-HIS < C14 < C16 when only enthalpies are considered. When considering the free energies, the order changes such that L-HIS < IMZ < BI < Me-IMZ << C14 < C16. That is, the superiority of the long chain inhibitors becomes more pronounced, and the role of the tail group in influencing the entropic factor changes the subtle differentiation between the smaller molecule imidazoles.

Table 5. Free Energy of adsorption (kJ/mol) of different corrosion inhibitors on to various metal hydroxide substrates at 298 K in presence of water. Binding Energies from Table 2 and log *P* values with reference to hexane from Table 3 are used.

Metal Hydroxide	Free Energy of Adsorption at 298 K (kJ/mol)					
	IMZ (A)	Me-IMZ (B)	BI (C)	L-HIS (D)	IMZ_C14 (E)	IMZ_C16 (F)
Cu(OH) ₂	−77	−78	−79	−47	−101	−112
Fe(OH) ₃	−70	−76	−73	−56	−	−
Al(OH) ₃	−142	−148	−146	−125	−183	−199
Ni(OH) ₂	−158	−159	−160	−136	−185	−195

In Table 5, the same kind of free energy analysis is performed as in Table 4, but using the hexane derived log *P* values. The binding free energies are not as strong in this case, given the change of reference solvent, but the trends remain the same.

4. Discussion

The key objective of this work was to explore the potential for using hydroxide clusters as simple models to enable fast analysis and generation of some parameters related to the effectiveness of potential inhibitor molecules to bind to hydroxylated surface films on various metals. The clusters studied—Ni(OH)₂, Cu(OH)₂, Al(OH)₃, and Fe(OH)₃—consist of a metal cation coordinated to two or three hydroxide species. The charge state of the clusters was overall neutral in charge, and the model inhibitors were considered to coordinate through the lone pair of electrons on the nitrogen atom in the imidazole unit. In such a representation, the metal clusters could resemble the undercoordinated exposed metal ions at the surface of an oxide film [38], or metal atoms that are coordinated to a hydroxylated surface of a metallic surface, which have been shown in prior work to have some partially cationic character [58]. Furthermore, the small metal hydroxide clusters studied herein are of the kind that has been proposed as a precursor to corrosion product formation [59]. As this brief discussion shows, there are different degrees as to which the cluster model can estimate each of the aforementioned cases, and further work would need to be done to draw some more quantitative similitudes. Similar analogies have been made to surface adsorption of oxygen as well as hydrogen to metal surfaces, where to some extent the adsorption energies, bond lengths and charge states have a semi-quantitative resemblance with their counterpart quantities in the solid-state oxide or hydride phases (i.e., adsorption energies, the scaled bulk formation energies, the bond lengths, the lattice parameters, the charge states, and the formal oxidation states in the ionic structures). Indeed, some of the first explorations of corrosion with quantum chemical techniques by Dr. Anderson in 1980 used cluster representations of Pt-H₂O and Fe-OH as surrogates for the surfaces [59].

Some fundamental electronic properties of the imidazoline derivatives studied herein were computed by density functional theory and reported by Kovacevic et al. in 2011 [39,60]. These parameters included the hardness, electronegativity, and dipole moment. For all three molecules, the values were similar with some differentiations. For hardness, imidazole > methylimidazole > benzimidazole; for electronegativity, benzimidazole > imidazole > methylimidazole; and for the dipole moments, methylimidazole > imidazole > benzimidazole. Hardness is relevant to the second derivative of the energy with respect to the charge, whereas electronegativity reflects the first-order derivative. The dipole moment reflects the electrostatic interaction. Generally, it is observed in the binding energies in Table 1 (which are most comparable to the data reported by Kovacevic [60] et al. that methylimidazole has the strongest binding, and imidazole the least strong, whereas, when there will be a complex interaction of these electronic trends, the predominance of methylimidazole suggests that the dipole moment contribution is a major factor. This seems reasonable because the interactions between the metal hydroxide clusters (which are neutral in charge, and do not involve the formation of covalent bonds) will be more on the level of physisorptions, and thus controlled by electrostatic effects as well as dispersion (which was not covered in this work, since the dispersion interactions are expected to be more considerable when

the broader molecular surface area is modeled to interact with a larger scale model for the metal or oxide surface).

The data reported herein can also be compared to some of the available experimental and theoretical literature available for the inhibitors and metal centers studied (or similar systems). Sun reported the adsorption energies of imidazole and benzimidazole on Cu(111) surface from density functional theory and found adsorption energies of -0.61 and -0.52 eV [61]. In the binding energies reported in Table 1, we find that the adsorption energies for the $\text{Cu}(\text{OH})_2$ cluster are stronger by a few tenths of an eV, and also that benzimidazole is slightly more strongly adsorbed than imidazole. Hence, hydroxylated copper ions appear to have a stronger affinity for the inhibitors than the unreacted elemental metallic copper surface.

Jiang et al. studied benzotriazole adsorption on $\text{Cu}_2\text{O}(111)$ surfaces and for low coverage obtained binding energies of -1.37 and -1.43 eV [62]. This surface will be more similar to the $\text{Cu}(\text{OH})_2$ case studied herein, where a binding energy of 107 (-1.1 eV) kJ/mol was found. Kovacevic et al. in 2011 found that imidazole had a binding energy of around -0.7 eV in the dilute limit of adsorption, and similarly for Al(111) (our value for imidazole on Al(111) is -1.5 eV and for Cu(111) is -1.1 eV) [39]. Thus, as anticipated in our preceding discussion, the use of a metal hydroxide cluster appears to be intermediate to that of the oxide surface and the metal surface in terms of comparative strength of adsorption.

A study by Mobin reported adsorption free energy values for L-histidine adsorption on mild steel at 0.1 M H_2SO_4 solution [63]. According to the Pourbaix diagram, the oxide is unstable in acidic conditions, although potentially some sub monolayer or monolayer film of water and/or hydroxide may be present on the surface [64]. The reported free energy of adsorption is -13 to -29 kJ/mol, based on a fitted isotherm model that relates the reduction in corrosion activity to the extent of surface coverage (which may not be an exact assumption). This adsorption free energy can be compared to the -87 or -56 kJ/mol as determined in this work (for the $\text{Fe}(\text{OH})_3$ model, with either *n*-octanol or hexane as the reference solvent for log *P*).

Mendes et al. used the DFT method with a slab model for the iron surface to compute adsorption energies for imidazole, but their adsorption energies are extremely high -569 kJ/mol for the perpendicular orientation on the surface [65]. The strongest binding energy reported in this work is around -200 kJ/mol, and a review of other studies of inhibitors reveals that this value by Mendes appears to be highly anomalous. On the other hand, Milosev et al. studied directly the adsorption of imidazole, methylimidazole and benzimidazole on Fe(110) and found adsorption energies of values -0.83 , -0.86 and -0.76 eV, respectively [66]. These values are about half of the binding strength of the values reported for $\text{Fe}(\text{OH})_3$ cluster in this work: -1.4 , -1.6 , -1.5 eV, respectively.

Feng et al. explore adsorption of imidazoline derivatives on Fe, Fe_3O_4 and Fe_2O_3 , reported binding energies of -284 kJ/mol, -157 kJ/mol and -226 kJ/mol [28]. These adsorption energies are considerably stronger ($2\times$) than from this work (-139 kJ/mol) for the $\text{Fe}(\text{OH})_3$ cluster. One significant reason for this is likely due to the long chains on the substituted imidazolines, which were laid out on the metal or oxide surfaces in the molecular dynamics model, thus contributing a large number of dispersion (van der Waals) interactions that, although small in individual value, can add up to a more considerable binding interaction.

Very little work has been done to examine the role of organic inhibitors on Al or Ni. A review of organic corrosion inhibitors for aluminum and aluminum alloys has recently been made available by Khanari [67]. Most of the references are quite new, indicating that this problem has become an increased topic of interest. As seen in the results presented in the present work, both Al and Ni have high free energies of adsorption for the inhibitors studied in this work, implying that organic chemical inhibitors may be extremely practical in these systems. However, the general review of inhibiting treatments in acidic environments by G. Schmitt covers a broad range of metals and compounds [68], and it was mentioned in that review that inhibitors that work well in iron and copper systems are less effective for Al and Ni. Unlike iron, Al and Ni both have highly corrosion resistant oxide films, and suffer

more from localized corrosion and stress-corrosion cracking, rather than uniform corrosion [69–71]. Therefore, it may be more important in these systems to study the interactions of inhibitors with critical defect sites in these oxide films, their ability to displace aggressive ions, such as chloride, and their adsorption on bare metallic surfaces that may be exposed in aggressive pitting environments. Typically for systems such as high-strength aluminum alloys, inorganic inhibitors have been used such as chromate and molybdate; however, concerns about their toxicity have led to a search for new, more environmentally friendly alternatives.

5. Conclusions

In this work, we have applied an innovative model for using first-principles modeling to infer thermodynamic properties related to the adsorption of inhibitor molecules onto metal centers. We have extended the original work by considering other metal centers, as well as performing some variations on the model decisions such as including the role of an aqueous environment, and considering the use of a solvent other than *n*-octanol for the partition coefficient. The results demonstrate that there is some sensitivity to these model choices, although generally the trends and predictions remain the same. The binding energies calculated by this method are intermediate between those reported for adsorption on metallic surfaces without defects or surface films, and those reported for adsorption on oxide surfaces. Whereas the results of this study are not conclusive, they provide some additional reference information for corrosion inhibitor properties with respect to copper and iron systems, as well as providing a basis for future work to explore the utility of organic corrosion inhibitors on metals and/or alloys containing aluminum and nickel.

In our opinion, the next extension of such studies should examine how the adsorption properties change as the metal cluster is expanded to include two, three or more metallic centers, thus building more reliable representations of an oxide film. In this way, what is the minimum number of metal centers required to obtain a converged solution to the problem of finding a minimum, irreducible unit for rapid screening of potential inhibitor molecular candidates could be determined. The inhibitor–inhibitor and inhibitor–solvent interactions will also need to be taken into account in more extended studies. Further validation of this model against experimental data is also required to determine how the free energies of adsorption from this model system may be scaled or otherwise interpreted to compare to ‘real world’ systems.

Acknowledgments: This work was supported by DNV GL, Dublin, OH, USA.

Author Contributions: Christopher D. Taylor conceived the study. Yathish Kurapati performed the calculations and generated the analysis and figures in this work. Sujit K. Mondal originated the methodology used. All authors contributed to the writing of the paper.

Conflicts of Interest: The authors declare no conflict of interest.

References

1. Obot, I.B. Recent advances in computational design of organic materials for corrosion protection of steel in aqueous media. In *Developments in Corrosion Protection*; Aliofkhaezraei, M., Ed.; Intech: London, UK, 2014.
2. Papavinasam, S. *Corrosion Control in the Oil and Gas Industry*; Elsevier: London, UK, 2014; p. 374.
3. Taylor, C.D.; Chandra, A.; Vera, J.; Sridhar, N. A Multiphysics Perspective on Mechanistic Models for Chemical Corrosion Inhibitor Performance. *J. Electrochem. Soc.* **2015**, *162*, C369. [[CrossRef](#)]
4. Gece, G. The use of quantum chemical methods in corrosion inhibitor studies. *Corros. Sci.* **2008**, *50*, 2981–2992. [[CrossRef](#)]
5. Durnie, W.; de Marco, R.; Jefferson, A.; Kinsella, B. Development of a Structure–Activity Relationship for Oil Field Corrosion Inhibitors. *J. Electrochem. Soc.* **1999**, *146*, 1751–1756. [[CrossRef](#)]
6. Ramakrishnan, S.K.; Martin, M.; Cloitre, T.; Firlej, L.; Gergely, C. Design rules for metal binding biomolecules: Understanding of amino acid adsorption on platinum crystallographic facets from density functional calculations. *Phys. Chem. Chem. Phys.* **2015**, *17*, 4193–4198. [[CrossRef](#)] [[PubMed](#)]

7. Khaled, K.F.; Sherik, A. Using neural networks for corrosion inhibition efficiency prediction during corrosion of steel in chloride solutions. *Int. J. Electrochem. Sci.* **2013**, *8*, 9918.
8. El Ashry, E.S.H.; el Nemr, A.; Essawy, S.A.; Ragab, S. Corrosion inhibitors part V: QSAR of benzimidazole and 2-substituted derivatives as corrosion inhibitors by using the quantum chemical parameters. *Prog. Organ. Coat.* **2008**, *61*, 11–20. [[CrossRef](#)]
9. El Ashry, E.S.H.; Senior, S.A. QSAR of lauric hydrazide and its salts as corrosion inhibitors by using the quantum chemical and topological descriptors. *Corros. Sci.* **2011**, *53*, 1025–1034. [[CrossRef](#)]
10. Lukovits, I.; Shaban, A.; Kalman, E. Thiosemicarbazides and thiosemicarbazones: Non-linear quantitative structure-efficiency model of corrosion inhibition. *Electrochim. Acta* **2005**, *50*, 4128–4133. [[CrossRef](#)]
11. Khalil, N. Quantum chemical approach of corrosion inhibition. *Electrochim. Acta* **2003**, *48*, 2635–2640. [[CrossRef](#)]
12. Arshadi, M.R.; Lashgari, M.; Parsafar, G.A. Cluster approach to corrosion inhibition problems: Interaction studies. *Mater. Chem. Phys.* **2004**, *86*, 311–314. [[CrossRef](#)]
13. Arslan, T.; Kandemirli, F.; Ebenso, E.E.; Love, I.; Alemu, H. Quantum chemical studies on the corrosion inhibition of some sulphonamides on mild steel in acidic medium. *Corros. Sci.* **2009**, *51*, 35–47. [[CrossRef](#)]
14. Du, L.; Zhao, H.; Hu, H.; Yang, J. Quantum chemical and molecular dynamics studies of imidazoline derivatives as corrosion inhibitor and quantitative structure-activity relationship (QSAR) analysis using the support vector machine (SVM) method. *J. Theor. Comp. Chem.* **2014**, *13*, 1450012. [[CrossRef](#)]
15. Plimpton, S.J. Fast Parallel Algorithms for Short-Range Molecular Dynamics. *J. Comp. Phys.* **1995**, *117*, 1. [[CrossRef](#)]
16. Kresse, G.; Furthmüller, J. Efficient Iterative Schemes for Ab initio Total-Energy Calculations Using a Plane-Wave Basis Set. *Phys. Rev. B* **1996**, *54*, 11169. [[CrossRef](#)]
17. Kresse, G. Furthmüller, Efficiency of ab-initio total energy calculations for metals and semiconductors using a plane-wave basis set. *J. Comput. Mat. Sci.* **1996**, *54*, 11169–11186.
18. Kresse, G.; Hafner, J. Ab initio molecular dynamics for liquid metals. *Phys. Rev. B* **1993**, *47*, 558–561. [[CrossRef](#)]
19. Finsgar, M.; Lesar, A.; Kokalj, A.; Milosev, I. A comparative electrochemical and quantum chemical calculation study of BTAH and BTAOH as copper corrosion inhibitors in near neutral chloride solution. *Electrochim. Acta* **2008**, *53*, 8287–8297. [[CrossRef](#)]
20. Peljhan, S.; Kokalj, A. DFT study of gas-phase adsorption of benzotriazole on Cu(111), Cu(100), Cu(110), and low coordinated defects thereon. *Phys. Chem. Chem. Phys.* **2011**, *13*, 20408–20417. [[CrossRef](#)] [[PubMed](#)]
21. Mondal, S.K.; Taylor, S.R. The identification and characterization of organic corrosion inhibitors: Correlation of a computational model with experimental results. *J. Electrochem. Soc.* **2014**, *161*, C476–C485. [[CrossRef](#)]
22. Kokalj, A. Is the analysis of molecular electronic structure of corrosion inhibitors sufficient to predict the trend of their inhibition performance? *Electrochim. Acta* **2010**, *56*, 745. [[CrossRef](#)]
23. Winkler, D.A.; Breedon, M.; Hughes, A.E.; Burden, F.R.; Barnard, A.S.; Harvey, T.G.; Cole, I. Towards chromate-free corrosion inhibitors: Structure-property models for organic alternatives. *Green Chem.* **2014**, *16*, 3349–3357. [[CrossRef](#)]
24. Winkler, D.A.; Breedon, M.; White, P.; Hughes, A.E.; Sapper, E.D.; Cole, I. Using high throughput experimental data and in silico models to discover alternatives to toxic chromate corrosion inhibitors. *Corros. Sci.* **2016**, *106*, 229–235. [[CrossRef](#)]
25. Chen, F.F.; Breedon, M.; Sapper, E.D.; Ganther, W.; Lau, D.; Cole, I. A microclimate model to simulate neutral salt spray testing for corrosion inhibitor evaluation and functional coating development. *Prog. Org. Coat.* **2017**, *111*, 327–335. [[CrossRef](#)]
26. Chen, F.F.; Breedon, M.; White, P.; Chu, C.; Mallick, D.; Thomas, S.; Sapper, E.D.; Cole, I. Correlation between molecular features and electrochemical properties using an artificial neural network. *Mater. Des.* **2016**, *112*, 410–418. [[CrossRef](#)]
27. Sangster, J. *Octanol-Water Partition Coefficients: Fundamentals and Physical Chemistry*; John Wiley & Sons: Chichester, UK, 1997.
28. Feng, L.J.; Yang, H.Y.; Wang, F.H. Experimental and theoretical studies for corrosion inhibition of carbon steel by imidazoline derivative in 5% NaCl saturated Ca(OH)₂ solution. *Electrochim. Acta* **2011**, *58*, 427–436. [[CrossRef](#)]

29. Blajiev, O.; Hubin, A. Inhibition of copper corrosion in chloride solutions by amino-mercapto-thiadiazol and methyl-mercapto-thiadiazol: An impedance spectroscopy and a quantum-chemical investigation. *Electrochim. Acta* **2004**, *49*, 2761–2770. [[CrossRef](#)]
30. Arrouvel, C.; Diawara, B.; Costa, D.; Marcus, P. DFT periodic study of the adsorption of glycine on the anhydrous and hydroxylated (0001) surfaces of alpha-alumina. *J. Phys. Chem. C* **2007**, *111*, 18164–18173. [[CrossRef](#)]
31. Borck, O.; Hyldgaard, P.; Schroder, E. Adsorption of methylamine on alpha-Al₂O₃(0001) and alpha-Cr₂O₃(0001): Density functional theory. *Phys. Rev. B* **2007**, *75*. [[CrossRef](#)]
32. Motta, A.; Gageot, M.P.; Costa, D. Ab Initio Molecular Dynamics Study of the AlOOH Boehmite/Water Interface: Role of Steps in Interfacial Grotthus Proton Transfers. *J. Phys. Chem. C* **2012**, *116*, 12514–12524. [[CrossRef](#)]
33. Gao, Y.Y.; Zhao, N.; Wei, W.; Sun, Y.H. Ab initio DFT study of urea adsorption and decomposition on the ZnO (10-1 0) surface. *Comput. Theor. Chem.* **2012**, *992*. [[CrossRef](#)]
34. Irrera, S.; Costa, D.; Ogle, K.; Marcus, P. Molecular modelling by DFT of 1,2-diaminoethane adsorbed on the Zn-terminated and O-terminated, anhydrous and hydroxylated ZnO (0001) surface. *Superlattices Microstruct.* **2009**, *46*, 19–24. [[CrossRef](#)]
35. Islam, M.M.; Diawara, B.; Marcus, P.; Costa, D. Synergy between ionic-covalent bonds and van der Waals interactions in SAMs formation: A first-principles study of adsorption of carboxylic acids on the Zn-ZnO(0001) surface. *Catal. Today* **2011**, *177*, 39–49. [[CrossRef](#)]
36. Tang, W.D.; Gao, Y.Y.; Wei, W.; Sun, Y.H. Adsorption of Urea onto a ZnO(10-10) Surface. *Acta Phys. Chim. Sin.* **2010**, *26*, 1373–1377.
37. Costa, D.; Marcus, P. Adsorption of Organic Inhibitor Molecules on Metal and Oxidized Surfaces Studied by Atomistic Theoretical Methods. In *Molecular Modeling of Corrosion Processes*; Taylor, C.D., Marcus, P., Eds.; ECS-Wiley: Hoboken, NJ, USA, 2015.
38. Kokalj, A.; Peljhan, S. Density Functional Theory Study of Adsorption of Benzotriazole on Cu₂O Surfaces. *J. Phys. Chem. C* **2015**, *119*, 11625–11635. [[CrossRef](#)]
39. Kovacevic, N.; Kokalj, A. DFT Study of Interaction of Azoles with Cu(111) and Al(111) Surfaces: Role of Azole Nitrogen Atoms and Dipole-Dipole Interactions. *J. Phys. Chem. C* **2011**, *115*, 24189–24197. [[CrossRef](#)]
40. Masel, R.I. *Principles of Adsorption and Reaction on Solid Surfaces*; Wiley: Hoboken, NJ, USA, 1996.
41. Levine, I.N. *Quantum Chemistry*; Prentice Hall: Upper Saddle River, NY, USA, 2000.
42. *Gaussian 09W*; Gaussian, Inc.: Wallingford, CT, USA, 2009.
43. Becke, A.D. Density-Functional Thermochemistry. III. The Role of Exact Exchange. *J. Chem. Phys.* **1993**, *98*, 5648–5652. [[CrossRef](#)]
44. Hay, P.J.; Wadt, W.R. Ab initio effective core potentials for molecular calculations. Potentials for the transition metal atoms Sc to Hg. *J. Chem. Phys.* **1985**, *82*, 270. [[CrossRef](#)]
45. Hay, P.J.; Wadt, W.R. Ab initio effective core potentials for molecular calculations. Potentials for main group elements Na to Bi. *J. Chem. Phys.* **1985**, *82*, 284.
46. Hay, P.J.; Wadt, W.R. Ab initio effective core potentials for molecular calculations. Potentials for K to Au including the outermost core orbitals. *J. Chem. Phys.* **1985**, *82*, 299. [[CrossRef](#)]
47. Cramer, C.J.; Truhlar, D.G. Density functional theory for transition metals and transition metal chemistry. *Phys. Chem. Chem. Phys.* **2009**, *11*, 10757–10816. [[CrossRef](#)] [[PubMed](#)]
48. Zhao, Y.; Truhlar, D.G. Density Functionals with Broad Applicability in Chemistry. *Acc. Chem. Res.* **2008**, *41*, 157–167. [[CrossRef](#)] [[PubMed](#)]
49. Zhao, Y.; Truhlar, D.G. Applications and validations of the Minnesota density functionals. *Chem. Phys. Lett.* **2011**, *502*, 1–13. [[CrossRef](#)]
50. Ramachandran, S.; Jovancevic, V. Molecular modeling of the inhibition of mild steel carbon dioxide corrosion by imidazolines. *Corros. Sci.* **1999**, *55*, 259–267. [[CrossRef](#)]
51. Thierry, D.; Leygraf, C. Enhanced Raman scattering of 1,2,4 triazole and imidazole adsorbed on microlithographically prepared copper surfaces. *J. Electrochem. Soc.* **1986**, *133*, 2236–2239. [[CrossRef](#)]
52. Martinez, J.A.; Yilmaz, D.E.; Liang, T.; Sinnott, S.B.; Phillpot, S.R. Fitting empirical potentials: Challenges and methodologies. *Curr. Opin. Solid State Mater. Sci.* **2013**, *17*, 263–270. [[CrossRef](#)]

53. Bukowska, J.; Kudelski, A.; Jockowska, K. The use of surface enhanced Raman scattering to prove the interaction of imidazole with the silver electrode surface. *J. Electroanal. Chem. Interfacial Electrochem.* **1991**, *309*, 251. [[CrossRef](#)]
54. Loo, B.H.; Tse, Y.; Parsons, K.; Adelman, C.; El-Hage, A.; Lee, Y.G. Surface-enhanced Raman spectroscopy of imidazole adsorbed on electrode and colloidal surfaces of Cu, Ag, and Au. *J. Raman Spectrosc.* **2006**, *37*, 299–304. [[CrossRef](#)]
55. Kovacevic, N.; Milosev, I.; Kokalj, A. How relevant is the adsorption bonding of imidazoles and triazoles for their corrosion inhibition of copper? *Corros. Sci.* **2017**, *124*, 25–34. [[CrossRef](#)]
56. Taylor, C.D.; Chandra, A.; Vera, J.; Sridhar, N. Design and prediction of corrosion inhibitors from quantum chemistry. II. A general framework for prediction of effective oil/water partition coefficients and speciation from quantum chemistry. *J. Electrochem. Soc.* **2015**, *162*, C347–C353. [[CrossRef](#)]
57. Marenich, A.V.; Cramer, C.J.; Truhlar, D.G. Universal Solvation Model Based on Solute Electron Density and on a Continuum Model of the Solvent Defined by the Bulk Dielectric Constant and Atomic Surface Tensions. *J. Phys. Chem. B* **2009**, *113*, 6378–6396. [[CrossRef](#)] [[PubMed](#)]
58. Taylor, C.D.; Kelly, R.G.; Neurock, M. A first-principles analysis of the chemisorption of hydroxide on copper under electrochemical conditions: A probe of the electronic interactions that control chemisorption at the electrochemical interface. *J. Electroanal. Chem.* **2007**, *607*, 167–174. [[CrossRef](#)]
59. Anderson, A.B.; Debnath, N.C. Mechanism of iron dissolution and passivation in an aqueous environment: Active and transition ranges. *J. Am. Chem. Soc.* **1983**, *105*, 18–22. [[CrossRef](#)]
60. Kovačević, N.; Kokalj, A. Analysis of molecular electronic structure of imidazole- and benzimidazole-based inhibitors: A simple recipe for qualitative estimation of chemical hardness. *Corros. Sci.* **2011**, *53*, 909–921. [[CrossRef](#)]
61. Sun, S.; Geng, Y.; Tian, L.; Chen, S.; Yan, Y.; Hu, S. Density functional theory study of imidazole, benzimidazole and 2-mercaptobenzimidazole adsorption onto clean Cu(111) surface. *Corros. Sci.* **2012**, *63*, 140–147. [[CrossRef](#)]
62. Jiang, Y.; Adams, J.B.; Sun, D.H. Benzotriazole adsorption on Cu₂O(111) surfaces: A first-principles study. *J. Phys. Chem. B* **2004**, *108*, 12851–12857. [[CrossRef](#)]
63. Mobin, M.; Parveen, M.; Rafiquee, M.Z.A. Inhibition of mild steel corrosion using L-histidine and synergistic surfactants additives. *J. Mater. Eng. Perform.* **2013**, *22*, 548–556. [[CrossRef](#)]
64. Deltombe, E.; de Zoubov, N.; Pourbaix, M. *Atlas of Electrochemical Equilibria in Aqueous Solution*; NACE: Houston, TX, USA, 1974.
65. Mendes, J.O.; da Silva, E.C.; Rocha, A.B. On the nature of inhibition performance of imidazole on iron surface. *Corros. Sci.* **2012**, *57*, 254–259. [[CrossRef](#)]
66. Milosev, I.; Kovacevic, N.; Kokalj, A. Electrochemical and Spectroscopic Study of Benzotriazole Films Formed on Copper, Copper-zinc Alloys and Zinc in Chloride Solution. *Acta Chim. Slov.* **2016**, *63*, 544–559. [[PubMed](#)]
67. Xhanari, K.; Finsgar, M. Organic corrosion inhibitors for aluminum and its alloys in chloride and alkaline solutions: A review. *Arabian J. Chem.* **2016**, in press. [[CrossRef](#)]
68. Schmitt, G. Application of inhibitors for acid media: Report prepared for the European Federation of Corrosion Working Party on Inhibitors. *Br. Corros. J.* **1984**, *19*, 165–176. [[CrossRef](#)]
69. Frankel, G.; Li, T.; Scully, J.R. Perspective—Localized corrosion: Passive film breakdown vs. pit growth stability. *J. Electrochem. Soc.* **2017**, *164*, C180–C181. [[CrossRef](#)]
70. Frankel, G.; Thornton, G.; Street, S.; Rayment, T.; Williams, D.; Cook, A.; Davenport, A.; Gibbon, S.; Engelberg, D.; Ornek, C.; et al. Localised corrosion: General discussion. *Faraday Discuss.* **2015**, *180*, 381–414. [[CrossRef](#)] [[PubMed](#)]
71. Frankel, G.S.; Scully, J.R.; Jahnes, C.V. Repassivation of pits in aluminum thin films. *J. Electrochem. Soc.* **1996**, *143*, 1834–1840. [[CrossRef](#)]

